ORIGINAL PAPER

T. Maly · L. Grgic · K. Zwicker · V. Zickermann
U. Brandt · T. Prisner

Cluster N1 of complex I from *Yarrowia lipolytica* studied by pulsed EPR spectroscopy

Abstract After reduction with nicotinamide adenine dinucleotide (NADH), NADH:ubiquinone oxidoreductase (complex I) of the strictly aerobic yeast *Yarrowia lipolytica* shows clear signals from five different paramagnetic iron–sulfur (FeS) clusters (N1–N5) which can be detected using electron paramagnetic resonance (EPR) spectroscopy. The ligand environment and the assignment of several FeS clusters to specific binding motifs found in several subunits of the complex are still under debate. In order to characterize the hyperfine interaction of the surrounding nuclei with FeS cluster N1, one- and two-dimensional electron spin echo envelope modulation experiments were performed at a temperature of 30 K. At this temperature only cluster N1 contributes to the overall signal in a pulsed EPR experiment. The hyperfine and quadrupole tensors of a nitrogen nucleus and the isotropic and dipolar hyperfine couplings of two sets of protons could be determined by numerical simulation of the one- and two-dimensional spectra. The values obtained are in perfect agreement with a ferredoxin-like binding structure by four cysteine amino acid residues and allow the assignment of the nitrogen couplings to a backbone nitrogen nucleus and the proton couplings to the β-protons of the bound cysteine residues.

T. Maly · T. Prisner (✉)
Institut für Physikalische und Theoretische
Chemie and Center for Biological Magnetic Resonance,
Johann-Wolfgang-Goethe-Universität Frankfurt,
60439 Frankfurt am Main, Germany
E-mail: prisner@chemie.uni-frankfurt.de
Fax: +49-69-79829404

L. Grgic · K. Zwicker · V. Zickermann · U. Brandt
Zentrum der Biologischen Chemie, Universitätsklinikum
Frankfurt, Molekulare Bioenergetik,
60590 Frankfurt am Main, Germany

Present address: T. Maly
Francis Bitter Magnet Laboratory and Department of Chemistry,
Massachusetts Institute of Technology,
Cambridge, MA 02139, USA

Introduction

NADH:ubiquinone oxidoreductase (complex I) of the mitochondrial respiratory chain is among the largest and most complicated membrane-bound multiprotein complexes known [1, 2] but currently little structural information is available. Complex I is the first complex of the mitochondrial respiratory chain and links the electron transfer from NADH to ubiquinone with the concomitant translocation of four protons across the inner membrane [3, 4]. Despite its central role in eukaryotic oxidative phosphorylation and its involvement in a broad range of human disorders [5], the function of the catalytic mechanism remains unclear.

Mitochondrial complex I is composed of some 40 different subunits with a total molecular mass of nearly 1,000 kDa [6] but smaller versions can be found in many bacteria [7]. Continuous-wave electron paramagnetic resonance (cw-EPR) experiments have demonstrated the presence of several iron–sulfur (FeS) clusters in complex I [8–10], although characterization of the individual paramagnetic centers is rather difficult owing to their similar spectroscopic properties. In general, complex I contains one molecule of non-covalently bound flavine mononucleotide and, depending on the organism, up to nine FeS clusters (2×[2Fe–2S] and 7×[4Fe–4S]) as electron transfer components [10], but until now only seven FeS clusters have been observed using EPR spectroscopy.

According to the nomenclature of complex I from bovine heart mitochondria the [2Fe–2S] clusters are designated N1a and N1b and the four detectable [4Fe–4S] clusters N2, N3, N4 and N5, corresponding to their temperature-dependent appearance in the cw-EPR spectrum [10]. Two more tetranuclear clusters, N6a and N6b, are found in subcomplexes or in the recombinant subunit [11, 12]. FeS cluster N7 is only observed in

prokaryotic complex I [12]. The arrangement of those clusters in the hydrophilic domain of complex I from *Thermus thermophilus* has recently been determined by X-ray crystallography [13]. At a resolution of 4 Å the structure shows that one binuclear cluster and six tetranuclear clusters are arranged in an 84-Å-long electron transfer chain. Clusters N1a and N7 do not participate in this pathway and are thought to play a role in the prevention of oxidative damage. Still, at this resolution the ligand environment and the assignment of the FeS clusters to specific binding motifs found in several subunits of the complex are not clear. In particular, it remains unclear how the three FeS clusters N1b, N4 and N5, which are bound to the 75-kDa subunit, are ligated by the three motifs found in the amino acid sequence [14, 15]. As a contribution to resolve this issue, we here focus on the analysis of the ligand environment of FeS cluster N1.

In this work we utilized the strictly aerobic yeast *Yarrowia lipolytica* as a model system for the analysis of mitochondrial complex I. At temperatures above 35 K, the typical spectrum of only one 2Fe–2S cluster (N1) is observed in isolated complex I from *Y. lipolytica* by cw-EPR spectroscopy. The spectroscopic properties of this center are similar to those reported for cluster N1b in the 75-kDa subunit of bovine complex I.

In contrast to cw-EPR experiments, it is possible to study cluster N1 separately from the other FeS clusters at a temperature of 30 K. This is due to the different relaxation behavior of the paramagnetic species in a pulsed EPR experiment (see "Discussion"). Although it is possible to study overlapping signals individually by pulsed EPR techniques (for example relaxation-filtered hyperfine (REFINE) electron spin echo envelope modulation (ESEEM) [16, 17]), here we used one-dimensional ESEEM and two-dimensional hyperfine sublevel correlation (HYSCORE) spectroscopy at 30 K in order to characterize the ^{1}H and ^{14}N interactions of FeS cluster N1 of mitochondrial complex I with its close vicinity. Since the hyperfine interaction of the electron spin with the nuclei in the close surrounding is usually hidden in the inhomogeneous line width of the EPR signal for such systems, ESEEM and HYSCORE spectroscopy are powerful tools to resolve these interactions [18].

Materials and methods

Complex I

The yeast *Y. lipolytica* is a powerful model for structural and functional analysis of complex I. It combines the availability of a purification protocol resulting in a pure, stable and enzymatically active complex I with the opportunity to use site-directed mutagenesis for functional and structural analysis [19, 20]. Growth of *Y. lipolytica* and preparation of affinity-purified complex I was performed as described elsewhere [21].

EPR samples were prepared using isolated complex I mixed with the physiological substrate nicotinamide adenine dinucleotide in its reduced form (NADH) directly in the EPR tube and were frozen in liquid nitrogen after 30-s reaction time. The cw-EPR spectrum from complex I reduced with NADH reveals signals originating from five different FeS clusters [22]. The tetranuclear clusters N2, N3, N4 and N5 are only observed at temperatures below 20 K, whereas cluster N1 can be observed up to a temperature of 60 K in a pulsed EPR experiment.

Instrumentation and methods

X-band spectra were measured with a Bruker E-580 spectrometer using a Bruker EPR cavity (MD5-W1) equipped with an Oxford Instruments helium-flow cryostat (CF935). The pulses were amplified using a 1-kW pulsed traveling wave tube amplifier. Field-swept spectra were obtained by integrating the area of a Hahn echo ($\pi/2 - \tau - \pi$) as a function of the magnetic field. For ESEEM [23] and HYSCORE [24] spectra the pulses were adjusted by optimizing the echo shape and intensity. Unwanted echoes were removed using an appropriate phase-cycle sequence [25]. All pulse lengths, timing and acquisition parameters are given in the respective figure caption.

Data analysis, processing and ^{14}N-ESEEM simulations

For ESEEM and HYSCORE experiments a background was subtracted from the time traces to remove the echo decay function. The remaining time traces were then multiplied by a Hanning window function and zero-filled to the double number of experimental data points. Magnitude Fourier spectra are shown in all cases.

Analysis of the ^{14}N hyperfine and quadrupole couplings using ESEEM and HYSCORE spectroscopy was done using the density matrix formalism [23]. Compared with $S = 1/2$, $I = 1/2$ systems, simulations of ESEEM traces due to ^{14}N nuclei require that the nuclear quadrupole interaction (nqi) is also taken into account. The additional term is given by

$$\widehat{H}_Q = \left(e^2 q Q / 4\right)\left[\left(3\widehat{I}_Z^{2'} - 2\right) + \eta\left(\widehat{I}_X^{2'} - \widehat{I}_Y^{2'}\right)\right]. \tag{1}$$

Five parameters are required to model the nuclear quadrupole interaction: $e^2 q Q / 4 = \kappa$, the quadrupole coupling constant; η the asymmetry parameter; and three Euler angles α, β and γ (the nuclear spin operators are primed because they refer to the nuclear quadrupole interaction principal axis system). The nuclear quadrupole Hamiltonian precludes the development of exact solutions for a modulation function and requires numerical simulations [26].

Results

Temperature dependence of the EPR signal

The field-swept spectra of complex I in a temperature range of 5–30 K are shown in Fig. 1. At 30 K only cluster N1 is visible in the EPR spectrum. By lowering the temperature, more and more clusters became visible. At 17 K cluster N2 also contributes to the EPR spectrum, while at 5 K four FeS clusters (N1–N4) are clearly visible in the absorption EPR spectrum (Fig. 1, bottom trace). Since some features are better visible in the first derivative of the EPR spectrum, a pseudomodulated spectrum was calculated in order to mimic a cw spectrum. These spectra are shown in Fig. 1 (right-hand side).

^{14}N interaction

At 30 K, three-pulse ESEEM measurements were performed on the EPR signal of cluster N1 (Fig. 2). Two different magnetic field positions were selected, corresponding to the $g_{||}$ (g_{zz}) and $g_{\perp}$ (g_{yy}/g_{xx}) principal values of the g tensor. In both cases slow modulations were observed, which were assigned to a nitrogen nucleus in close vicinity of cluster N1. After processing the experimental data and Fourier transformation of the time traces, the ESEEM spectra recorded at a field position corresponding to $g_{||}$ and $g_{\perp}$ show several peaks—most prominent at frequencies of 1.1, 1.9, 3.1 and 4.3 MHz ($g_{||}$) and at 1.7, 2.3, 3.1, 4.0 and 4.4 MHz ($g_{\perp}$).

In order to simplify the analysis of the peaks observed in the ESEEM spectra, two-dimensional HYSCORE spectroscopy was used, where correlations between two nuclear frequencies of different manifolds can be observed. Figure 3 shows the HYSCORE spectrum of cluster N1 taken at a field position corresponding to $g_{\perp}$ of the axial g tensor. Several correlations, which are only visible in the $(+, +)$ quadrant, were observed. The most prominent correlations are at the frequency positions (4.0/2.3), (4.0/3.1), (3.1/4.0) and (2.3/4.0) MHz. These correlations can be assigned to a double quantum–double quantum (dq–dq) and a single quantum–double quantum (sq–dq) correlation, respectively. Since no more features are visible, the resonances are thought to arise from an interaction of the electron spin with a single ^{14}N nucleus.

^{1}H interaction

Beside the ^{14}N interaction also modulations due to hyperfine interactions with protons were observed in the HYSCORE time traces taken at a field position corresponding to $g_{\perp}$ of cluster N1. After Fourier transformation two wing-shaped features in the ^{1}H region were observed in the HYSCORE spectrum. The HYSCORE spectrum, recorded at the maximum EPR signal intensity, is shown in Fig. 4. The same features were observed
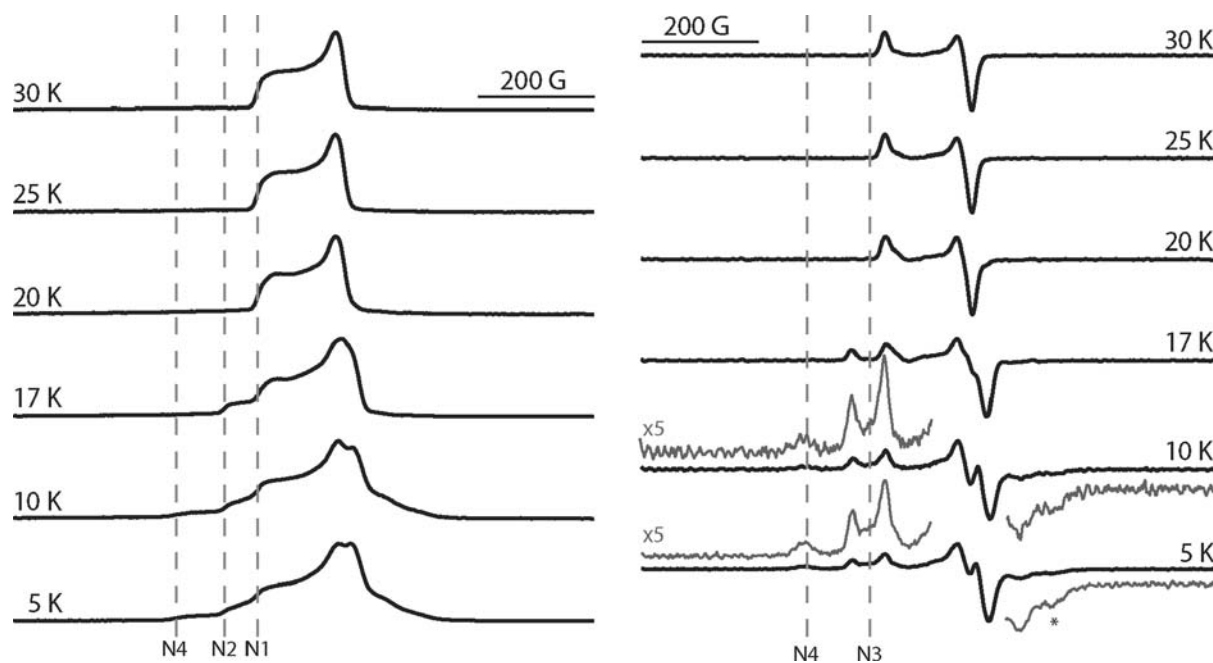
Fig. 1 Temperature dependence of the electron paramagnetic resonance spectra of complex I from *Yarrowia lipolytica*. *Left*: absorption spectra taken with a two-pulse field-swept sequence at the temperatures as indicated. *Right*: pseudomodulated spectra (10 G) of the absorption spectra shown on the *left*. The $g_{||}$ components of the iron–sulfur clusters N1–N4 are indicated by *dashed lines*. The g_{xx} component of cluster N3 is indicated by an *asterisk*. Experimental parameters, $t_p(\pi/2) = 12$ ns, $\tau = 140$ ns
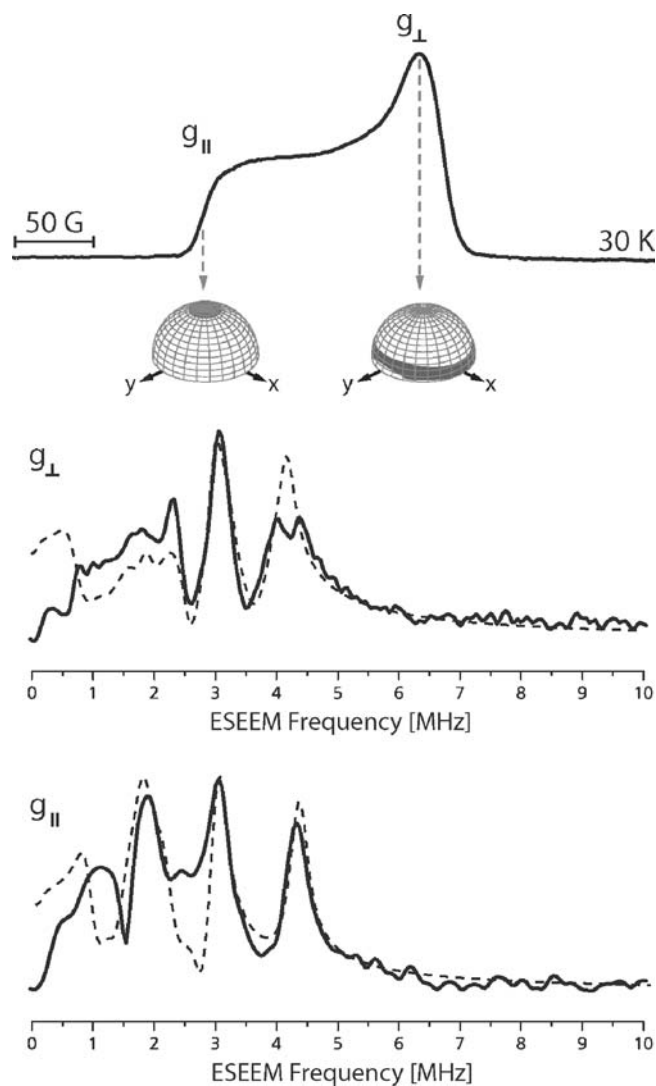
Fig. 2 *Top*: field-swept spectrum of complex I at 30 K. The two principal *g* values of cluster N1 are indicated and the respective orientation selection is shown on the sphere (hyperfine and quadrupole interactions neglected). *Middle and bottom*: three-pulse electron spin echo envelope modulation (*ESEEM*) spectra of cluster N1 recorded at a magnetic field corresponding to $g_\perp$ (*middle*) and $g_\parallel$ (*bottom*) and their respective simulations (*dashed line*). Experimental parameters, $t_p(\pi/2) = 12$ ns, $\tau = 132$ ns, $T = 0$–5.12 μs (256 points), 630 scans are taken with 100 shots per loop. Simulation parameters are given in Table 1

in samples where the medium was exchanged to D_2O (spectrum not shown).

Discussion

Temperature dependence of the EPR signal

At low temperatures (below 5 K) up to five different FeS clusters are clearly visible in the cw-EPR spectrum of complex I from *Y. lipolytica*, and the 35 and 12 K spectra of the isolated complex were found to be similar
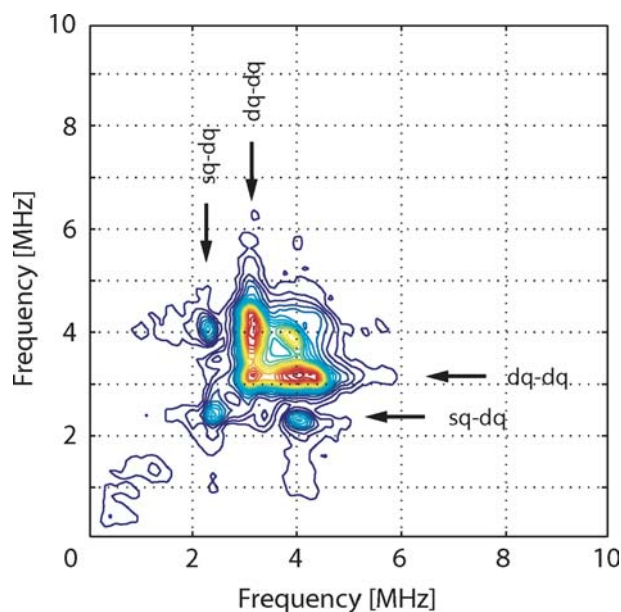
Fig. 3 ^{14}N hyperfine sublevel correlation (*HYSCORE*) spectrum of complex I at 30 K taken at a field position corresponding to $g_\perp(N1)$. Only the $(+,+)$ quadrant is shown. Two correlation peaks are indicated by *arrows* (*sq* single quantum, *dq* double quantum). Experimental parameters, $t_p(\pi/2) = 12$ ns, $t_p(\pi) = 8$ ns, $\tau = 152$ ns, $T = 0$–5.98 μs (300 points) in both dimensions, a single scan is taken with 170 shots per loop

to cw-EPR spectra reported earlier for the *Neurospora crassa* enzyme and *Y. lipolytica* [22, 27].

However, the temperature dependence of the EPR signals of the FeS clusters in a two-pulse echo-detected field-swept experiment can be very different from that in a cw experiment. While the relaxation behavior of the cw signal is given by $(T_1 T_2)^{-1}$, the two-pulse echo intensity is mainly affected by the fast relaxation times T_2 of the FeS clusters. Since T_1 and T_2 can be very different, the relaxation-weighted field-swept spectra can be completely different from the cw-EPR spectra. This can be seen in the temperature dependence of the EPR signal resulting from the different relaxation behavior of the FeS clusters.

For example, at 17 K only two FeS clusters are detected in the pulsed experiment (Fig. 1), whereas in a cw-EPR spectrum at this temperature, already four FeS clusters contribute to the EPR spectrum (data not shown). At 5 K four FeS clusters are visible in the EPR spectrum.[1]

Under these experimental conditions ($t = 140$ ns), the tetranuclear FeS cluster N5 could not be detected unambiguously owing to the overlap with the clusters N1–N4. It is known from cw-EPR spectroscopy that this FeS cluster is only visible at low temperatures (below 5 K) and high microwave power [22], suggesting that

---

[1]Although some resonances are difficult to detect [$g_{zz}(N3)$] the EPR spectrum at 5 K shows the same features as the cw-EPR spectra previously recorded and cluster N3 can be clearly identified by its g_{xx} component (indicated by the asterisk in Fig. 1).
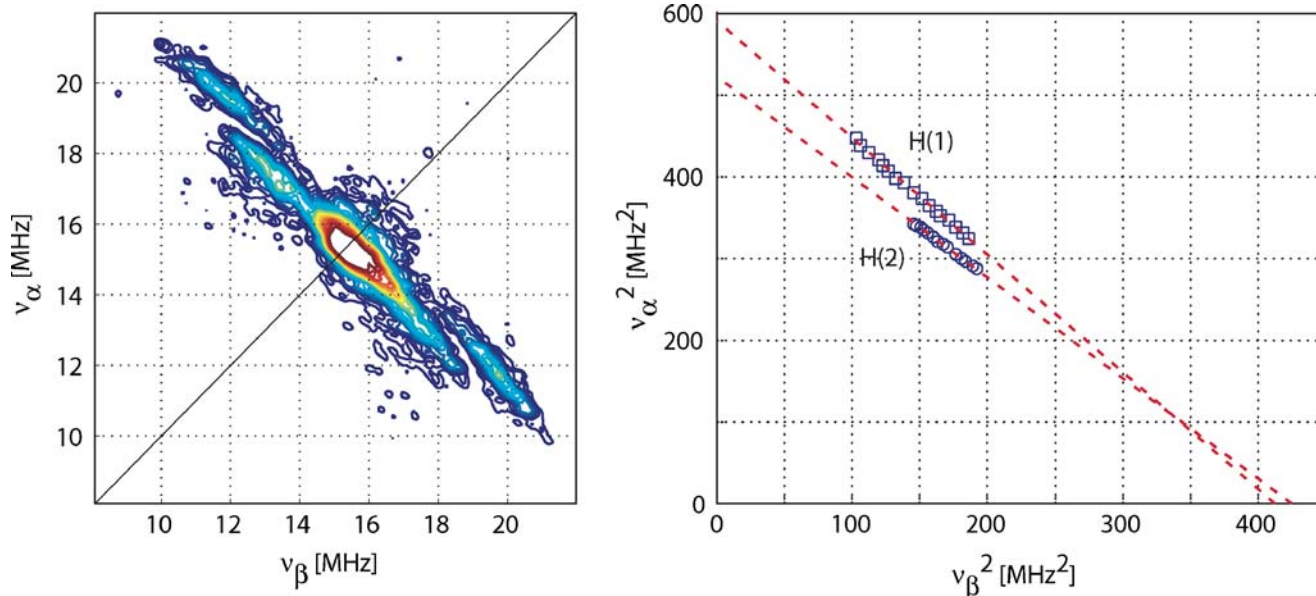
Fig. 4 *Left*: ^{1}H-HYSCORE spectrum of complex I at 30 K taken at a field position corresponding to g_{xy}(N1). Only the $(+,+)$ quadrant is shown. Experimental parameters, $t_p(\pi/2) = 12$ ns, $t_p(\pi) = 8$ ns, $\tau = 132$ ns, $T = 0$–3.072 μs (256 points) in both dimensions, one scan is taken with 170 shots per loop. *Right*: Selected points on the ridge of the HYSCORE spectrum shown on the *left*. The points are presented in a squared-axes representation (for more information see text)

this cluster has very short relaxation times. Therefore, the contribution of this FeS cluster to the overall EPR signal is most probably very small. In order to study cluster N1 separately from all other FeS clusters, pulsed EPR experiments can be performed at 30 K.

One- and two-dimensional ESEEM spectroscopy of cluster N1

EPR spectra of FeS clusters are usually very broad, since the g tensor of these paramagnetic species shows a large anisotropy [28, 29]. In fact, in case of frozen biological samples, with randomly distributed orientations of the protein with respect to the external magnetic field, it is often not possible to excite the whole EPR spectrum, owing to the limited excitation bandwidth of the microwave pulses. However, this provides the possibility to record single-crystal-like EPR spectra. If the g tensor is known and the hyperfine and quadrupole interactions can be neglected, the excited orientations can be easily calculated, leading to a subensemble of molecules with specific orientations with respect to the external magnetic field. This is shown in Fig. 2, where the excited orientations are indicated in dark gray on a unit sphere within the molecular g-axis system. At 30 K and a field position corresponding to $g = 2.02$ mainly FeS clusters with their $g_{||}$ components oriented along the external magnetic field direction are selected. If the pulsed EPR experiment is performed at a magnetic field corresponding to $g = 1.94$, only paramagnetic centers with their g_{zz} axis perpendicular with respect to the external magnetic field are excited.

The shift in the ESEEM transition frequencies observed as a function of the magnetic field value (data not shown) is proportional to the gyromagnetic ratio of ^{14}N and therefore indicates that the observed transitions were caused by a ^{14}N nucleus interacting with cluster N1. In principle, up to six transitions for each coupled nucleus can be observed but usually this number is reduced since some transition frequencies are strongly orientation dependent or have small transition moments. Even in the case of an ESEEM spectrum recorded at a magnetic field corresponding to $g_{||}$ only four peaks were observed. For quantitative analysis, the observed transitions had to be assigned to the different nuclear transitions within the nuclear manifolds (nuclear sq or dq transitions). This assignment was easily done in a HYSCORE experiment using similar experimental conditions as in the three-pulse ESEEM experiment. Because of the limited signal-to-noise ratio, it was only possible to record a proper HYSCORE spectrum for the $g_{\perp}$ position.

The HYSCORE spectrum in Fig. 3 strongly indicated that only a single nitrogen nucleus is coupled to FeS cluster N1. Following the analysis given in Ref. [30] the most dominant peaks at the frequencies (4.0/3.1) and (3.1/4.0) MHz were assigned to the dq–dq correlation peaks, whereas the frequency pair at (4.0/2.3) and (2.3/4.0) MHz could be assigned to a sq–dq correlation. In principle, up to 18 correlation peaks can be observed in a HYSCORE spectrum of a single ^{14}N nucleus, but as in the one-dimensional ESEEM experiment, typically only a subset of these correlations can be detected in the experiment because some of them have negligible intensities, are too broad or are suppressed by blind

spots. Since in our case the ESEEM spectrum only showed three strong peaks, the maximum number of expected correlation peaks in the HYSCORE spectrum was also reduced. By comparing the simulated HYSCORE patterns (given in Ref. [30]) for some typical configurations of nitrogen nuclei coordinated to an FeS cluster (hyperfine and quadrupole parameters), we could assume the case of a weakly bound nitrogen coordinated to cluster N1. This was also confirmed by the fact that no correlation peaks appeared in the $(+, -)$ quadrant.

Numerical simulations based on the modulation formula of Bowman and Massoth [26] were performed to confirm these results using a self-written routine. For the simulation one nitrogen nucleus was used to simulate the ESEEM spectrum simultaneously for both different orientation selections. The simulation parameters obtained are given in Table 1. It turned out that the positions of the peaks were mainly given by the values of A, Q and η, while the amplitudes were very sensitive to the Euler angles of the respective interaction tensors.

Since no atomic model of complex I is available so far, also the nature of the associated nitrogen nucleus is unknown. Two different types of coordination are typical for [2Fe–2S] clusters, namely, a Rieske-type or a ferredoxin-type structure. Both coordination types have their own characteristic frequency patterns in the ESEEM spectrum. For example, even before the crystal structure of the cytochrome bc_1 complex was known, it could be shown by electron–nuclear double resonance [31, 32] and ESEEM [33, 34] spectroscopy that the Rieske center has a different coordination environment, namely, two directly coordinated histidine residues. Until then, only ferredoxin-type coordination was known, where four cysteine residues coordinate the FeS cluster and the ^{14}N hyperfine interactions arise from backbone nitrogen atoms in close vicinity of the FeS cluster.

The two different coordination types, ferredoxin-type and Rieske-type, show clear differences in their quadrupole and hyperfine parameters. For nitrogen nuclei coordinated directly to the [2Fe–2S] cluster (Rieske-type) the hyperfine couplings of the distal nitrogen of the histidine are in the range 4–5 MHz and the quadrupole

coupling constant Q is below 3 MHz. This usually gives two sharp lines in the ESEEM spectrum around 4 and 7 MHz. and is called the "strongly coupled" case. In the case of ferredoxins the nitrogen hyperfine signal is caused by the interaction of a backbone nitrogen nucleus with the FeS cluster. This backbone nitrogen is typically located in a distance of 2–3 Å and the isotropic ^{14}N hyperfine value is usually in the range of 1 MHz and the quadrupole coupling constant is in the range of 3.3 MHz. In this case the nitrogen is "weakly coupled".

Some hyperfine and quadrupole coupling parameters of ^{14}N nuclei coordinated to [2Fe–2S] clusters for the Rieske-type and the ferredoxin-type of different organisms are collected in Table 2 and plotted in Fig. 5. From Fig. 5, two separate domains can be distinguished (dashed circles). The values for cluster N1 are indicated in the same figure by the asterisk and clearly show that cluster N1 is a ferredoxin-type bound [2Fe–2S] FeS cluster interacting with a backbone nitrogen nucleus. It can be assumed that cluster N1 corresponds to cluster N1b known from bovine and bacterial complex I and is therefore located in the 75-kDa subunit. This subunit also ligates FeS clusters N4 and N5 [14], but contains only 11 conserved cysteine residues. A conserved histidine has been proposed as the fourth ligand of cluster N5 [14], but it has been shown that removing this residue had no effect on the EPR spectrum of this redox center [15]. On the basis of our results, it can be excluded that a histidine or any other nitrogen ligand is involved in binding FeS cluster N1.

In the ^{1}H region of the HYSCORE spectra of cluster N1 large features were observed, and these also remained after changing the medium from H_2O to D_2O.

Table 1 Simulation parameters used to simulate electron spin echo envelope modulation spectra of cluster N1

Simulation parameter	Value
(A_{xx}, A_{yy}, A_{zz})	(0.5, 0.9, 1.2) MHz
a_{iso}	0.9 MHz
$\alpha^A, \beta^A, \gamma^A$	0°, 160°, 60°
Q	3.1 MHz
η	0.5
$\alpha^Q, \beta^Q, \gamma^Q$	30°, 50°, 0°

In the case of axial symmetric interaction tensors, the angle γ can be neglected. Since this is not the case here, all three Euler angles have to be taken into account. The errors for the hyperfine and quadrupole values were estimated to be ± 0.1 MHz. The errors of the Euler angles were estimated to be $\pm 10°$

Table 2 Hyperfine and quadrupole coupling parameters of ^{14}N nuclei coordinated to [2Fe–2S] centers of different enzymes

	A_{iso} (MHz)	Q (MHz)	Reference
Rieske or Rieske-type			
Bovine heart mitochondrial membranes	3.55	2.25	[34]
	5.20	2.93	
Cytochrome $b_6 f$ (spinach)	4.58	2.70	[33]
	3.75	2.70	
Burkholderia cepacia	3.70	2.15	[41]
	4.70	(3.85)[a]	
B. cepacia AC 1100	3.87	2.40	[31]
	4.90	2.32	
Pseudomonas putida	3.56	2.43	[42]
	4.78	2.31	
Ferredoxin or ferredoxin-type			
P. putida	1.11	3.27	[42]
Clostridium pasteurianum	0.61	3.29	[43]
Arum maculatum	1.10	3.32	[34]
Spirulina platensis	1.01	3.52	[34]
Escherichia coli (reduced)	1.06	3.41	[34]
E. coli (oxidized)	1.10	3.30	[44]
Porphyra umbilicalis	1.16	3.24	[45]
	0.40	3.04	

For Rieske-type coordination, only the value of the remote nitrogen is given here. All quadrupole couplings are given for $\eta = 0.5$
[a] This value is unusually high and was excluded from the analysis
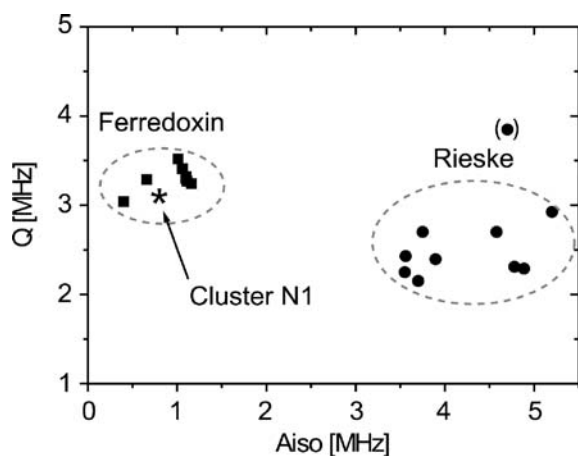
Fig. 5 Hyperfine and quadrupole parameters of different [2Fe–2S] clusters of metalloproteins. Values taken form Table 2. The *circles* indicate the two different types of coordination referred to as Rieske-type and ferredoxin-type. The hyperfine and quadrupole coupling constants determined for a ^{14}N interacting with cluster N1 are indicated by the *asterisk*

Table 3 Anisotropic and isotropic hyperfine couplings of β-protons as determined from the hyperfine sublevel correlation spectrum

Proton	Slope	Intercept	Hyperfine values	
	Q_α	G_α (MHz^2)	A_{iso} (MHz)	T (MHz)
H(1)	−1.43	590.56	(−8.4) 2.4	6.0
H(2)	−1.23	522.31	(−4.9) 1.4	3.5

The error of the hyperfine values determined is about ±0.5 MHz. Hyperfine values with the opposite sign are given in *parentheses* (see text)

These features were assigned to two pairs of resolved cross-peaks of β-protons of cysteine residues ligated to cluster N1, having strong hyperfine interactions. The contour line shape for a proton ($I = 1/2$) coupled to an electron spin ($S = 1/2$) by an axial hyperfine interaction in an orientationally disordered sample is described by [35, 36]

$$v_\alpha = \left(Q_\alpha v_\beta^2 + G_\alpha \right)^{1/2}, \tag{2}$$

with

$$Q_\alpha = \frac{(T + 2a - 4v_I)}{(T + 2a + 4v_I)}, \tag{3}$$

and

$$G_\alpha = 2v_I \frac{\left(4v_I^2 - a^2 + 2T^2 - aT\right)}{(T + 2a + 4v_I)}. \tag{4}$$

Thus, when plotting the HYSCORE spectra in a coordinate system with squared axes, the wing shape of the contour line is transformed into a straight line. It is then possible to calculate the isotropic hyperfine value (a) and the dipolar part (T) of the proton hyperfine tensor from the slope (Q_α) and the intercept (G_α) in this representation. One big advantage of this analysis is that even in the case of partial excitation and suppression artifacts caused by blind spots it is possible to determine the hyperfine coupling constants.

For the ^{1}H-HYSCORE spectrum of cluster N1 taken at a field position corresponding to g_{xy} several points were collected following the maximum contour level of the ridges above the diagonal (Fig. 4, left). These points were then plotted in a figure with squared axes and a linear regression was performed through each individual set of protons (Fig. 4, right). The values obtained are given in Table 3. Since it was not possible to determine

the sign of the hyperfine coupling, it was assumed that the isotropic hyperfine value of every β-proton had the same sign as the maximum component of the hyperfine tensor [37, 38]. Both sets of parameters fulfill these conditions and isotropic hyperfine values of 2.5 and 1.4 MHz and dipolar values of 6.0 and 3.5 MHz, respectively, can be determined. These values are in the range of typical values for β-protons of cysteines [37, 39, 40]. From this analysis only two set of protons could be identified, but in fact it is a moot point whether more information from the ^{1}H-HYSCORE spectrum can be obtained since the resolution is not good enough and no other geometrical information about the ligand sphere of cluster N1 is available.

Conclusions

Hyperfine spectroscopy, especially HYSCORE, is a very powerful tool to determine the local protein structure around paramagnetic centers. For metal centers which usually show a large anisotropy of the g tensor the selection of specifically oriented molecules with respect to the external magnetic field allows us to obtain not only the main values of the hyperfine and quadrupole tensors but also their orientations with respect to the molecular axis system in disordered protein samples. This information can be used as a fingerprint signature to assign the structure and binding geometry of the paramagnetic center to specific classes by comparison or can directly be related to local structure by quantum chemical calculations. We could separate and determine the isotropic and dipolar hyperfine couplings of two sets of protons and the hyperfine and quadrupole tensor values of a close-by nitrogen nucleus. Comparison with hyperfine data from other FeS clusters revealed that the hyperfine spectra of N1 are very similar to those of ferredoxin-type FeS clusters and allowed us to assign the nitrogen coupling to a backbone nitrogen nucleus and the proton hyperfine couplings to two sets of β-protons of the cysteine ligands.

References

1. Videira A (1998) Biochim Biophys Acta 1364:89–100
2. Brandt U, Kerscher S, Dröse S, Zwicker K, Zickermann V (2003) FEBS Lett 545:9–17
3. Wikström MKF (1984) FEBS Lett 169:300–304
4. Weiss H, Friedrich T (1991) Biochim Biophys Acta 23:743–771
5. Shapira AH (1998) Biochim Biophys Acta 1364:261–270
6. Hirst J, Carroll J, Fearnley IM, Shannon J, Walker JE (2003) Biochim Biophys Acta 1604:135–150
7. Yagi T, Yano S, Di Bernado S, Matsuno-Yagi A (1998) Biochim Biophys Acta 1354:125–133
8. Yano T, Ohnishi T (2001) J Bioenerg Biomemb 33:213–222
9. van Belzen R, Kotlyar AB, Moon N, Dunham WR, Albracht SPJ (1997) Biochemistry 36:886–893
10. Ohnishi T (1998) Biochim Biophys Acta 1364:186–206
11. Rasmussen T, Scheide D, Brors B, Kintscher L, Weiss H, Friedrich T (2001) Biochemistry 40:6124–6131
12. Nakamaru-Ogiso E, Yano T, Yagi T, Ohnishi O (2005) J Biol Chem 280:301–307
13. Hinchliffe P, Sazanov LA (2005) Science 309:771–774
14. Yano T (2003) J Biol Chem 278:15514–15522
15. Waletko A, Zwicker K, Abdrakhmanova A, Zickermann V, Brandt U, Kerscher S (2005) J Biol Chem 280:5622–5625
16. Maly T, MacMillan F, Zwicker K, Kashani-Poor N, Brandt U, Prisner T (2004) Biochemistry 43:3969–3978
17. Maly T, Prisner T (2004) J Magn Reson 170:88–96
18. Deligiannakis Y, Louloudi M, Hadjiliadis N (2000) Coord Chem Rev 204:1–112
19. Kerscher S, Dröse S, Zwicker K, Zickermann V, Brandt U (2002) Biochim Biophys Acta 1555:83–91
20. Dröse S, Zwicker K, Brandt U (2002) Biochim Biophys Acta 1556:65–72
21. Kashani-Poor N, Kerscher S, Zickermann V, Brandt U (2001) Biochim Biophys Acta 1504:363–370
22. Djafarzadeh R, Kerscher S, Zwicker K, Rademacher M, Lindahl M, Schägger H, Brandt U (2000) Biochim Biophys Acta 1459:230–238
23. Mims WB (1972) Phys Rev B 5:2409–2419
24. Höfer P, Grupp A, Nebenführ H, Mehring M (1986) Chem Phys Lett 132:279–282
25. Gemperle C, Aebli G, Schweiger A, Ernst RR (1990) J Magn Reson 88:241–256
26. Bowman MK, Massoth RJ (1987) In: Weil JA (ed) Electron magnetic resonance of the solid state. The Canadian Society for Chemistry, Ottawa, pp 99–110
27. Wang D-C, Meinhardt SW, Sackmann H, Weiss H, Ohnishi T (1991) Eu J Biochem 197:257–264
28. Mouesca J-M, Lamotte B (1998) Coord Chem Rev 178–180:1573–1614
29. Noodelman L, Lovell T, Liu T, Himo F, Torres RA (2002) Curr Opin Chem Biol 6:259–273
30. Dikanov SA, Xun L, Karpiel AB, Tyryshkin AM, Bowman MK (1996) J Am Chem Soc 118:8408–8416
31. Gurbiel RJ, Batie CJ, Sivaraja M, True AE, Fee JA, Hoffmann BM, Ballou DP (1989) Biochemistry 28:4861–4871
32. Gurbiel RJ, Ohnishi T, Robertson DE, Daldal F, Hoffmann BM (1991) Biochemistry 30:11579–11584
33. Britt RD, Sauer K, Klein MP, Knaff DB, Kriauciunas A, Yu CA, Yu L, Malkin R (1991) Biochemistry 30:1892–1901
34. Shergill JK, Cammack R (1994) Biochim Biophys Acta 1185:43–49
35. Dikanov SA, Bowman MK (1995) J Magn Reson A 116:125–128
36. Dikanov SA, Tyryshkin AM, Bowman MK (2000) J Magn Reson 144:228–242
37. Dikanov SA, Bowman MK (1998) J Biol Inorg Chem 3:18–29
38. Mouesca J-M, Rius G, Lamotte B (1993) J Am Chem Soc 115:4714–4731
39. Canne C, Ebelshäuser M, Gay E, Shergill JK, Cammack R, Kappl R, Hütermann J (2000) J Biol Inorg Chem 5:514–526
40. Kappl R, Ciurli S, Luchinat C, Hütermann J (1999) J Am Chem Soc 121:1925–1935
41. Riedel A, Fetzner S, Rampp M, Lingens F, Liebl U, Zimmermann J-L, Nitschke W (1995) J Biol Chem 270:30869–30873
42. Shergill JK, Joannou CL, Mason JR, Cammack R (1995) Biochemistry 34:16533–16542
43. Shergill JK, Golinelli M-P, Cammack R, Meyer J (1996) Biochemistry 35:12842–12848
44. Cammack R, Chapman A, McCracken J, Peisach J (1991) J Chem Soc Faraday Trans 87:3203–3206
45. Dikanov SA, Tyryshkin AM, Felli I, Reijerse EJ, Hütermann J (1995) J Magn Reson 108:99–102